7-19-2005

The discretized Schrödinger equation for the finite square well and its relationship to solid-state physics

Timothy B. Boykin
Electrical and Computer Engineering, University of Alabama

Gerhard Klimeck
Network for Computational Nanotechnology, Electrical and Computer Engineering, Purdue University, gekco@purdue.edu

INSTITUTE OF PHYSICS PUBLISHING EUROPEAN JOURNAL OF PHYSICS

Eur. J. Phys. **26** (2005) 865–881 doi:10.1088/0143-0807/26/5/020

The discretized Schrödinger equation for the finite square well and its relationship to solid-state physics

Timothy B Boykin[1] **and Gerhard Klimeck**[2]

[1] Department of Electrical and Computer Engineering, The University of Alabama in Huntsville, Huntsville, AL 35899, USA
[2] Network for Computational Nanotechnology, School of Electrical and Computer Engineering, Purdue University, West Lafayette, IN 47907, USA

Received 11 February 2005, in final form 29 April 2005
Published 19 July 2005
Online at stacks.iop.org/EJP/26/865

Abstract

The discretized Schrödinger equation is most often used to solve one-dimensional quantum mechanics problems numerically. While it has been recognized for some time that this equation is equivalent to a simple tight-binding model and that the discretization imposes an underlying bandstructure unlike free-space quantum mechanics on the problem, the physical implications of this equivalence largely have been unappreciated and the pedagogical advantages accruing from presenting the problem as one of solid-state physics (and not numerics) remain generally unexplored. This is especially true for the analytically solvable discretized finite square well presented here. There are profound differences in the physics of this model and its continuous-space counterpart which are direct consequences of the imposed bandstructure. For example, in the discrete model the number of bound states plus transmission resonances equals the number of atoms in the quantum well.

1. Introduction

For all but the simplest potentials, the one-dimensional Schrödinger equation admits only numerical solutions. The wavefunction and potential are typically sampled at discrete, evenly spaced points along the axis and the second derivative of the wavefunction is replaced by its centred-difference approximation. The resulting discretized equation is equivalent to that which results from a single-band tight-binding model [1]. The discretized model has been used to find the Bloch states of bulk semiconductors [1] as well as the bound states of both the infinite [2] and symmetric finite quantum wells [3]. The discrete model may therefore be viewed in physical [2] or purely mathematical [3] terms.

An essential feature of the discretized model, regardless of the point-of-view taken, is the energy bandstructure imposed on the model and resulting solutions by the discretization itself.

These solutions are no longer the same as those of continuous quantum mechanics and can only be correctly interpreted in terms of the imposed bandstructure. In mathematical terms, this bandstructure is a numerical fact which must be used to calculate eigenvalues. In physical terms, the discretization is actually desirable, because many physical systems (e.g., quantum wells) are fabricated from crystalline semiconductors. Because the spacing between atoms in a semiconductor is finite, as is the bandwidth of the energy bands, the discretized model is therefore closer to the true physics than is the continuous one.

When presented in physical terms, the discretized treatment also has a pedagogical advantage in that it serves as an introduction to more realistic, multi-band tight-binding nanostructure models. These multi-band models are very powerful and can handle a great variety of nanostructures, such as molecular electronic devices and quantum wells, wires and dots [4–10]. Electromagnetic fields can also be incorporated permitting the calculation of the dielectric constant and magnetotunnelling characteristics [11–13]. However, the matrix formulation of these models can be difficult for students. For example, the sp^3s^* model [14] for bulk has a 10×10 Hamiltonian matrix. Because the matrices of multi-band models usually require numerical solution, presenting the discretized Schrödinger equation as a tight-binding model and relating its analytic solutions to elementary continuous quantum mechanics can bridge this gap for students.

Earlier work [2] shows how the imposed bandstructure greatly affects the solutions of the discrete model. For example, with infinite barriers the number of atoms in the quantum well determines the number of bound states. Similar effects occur for the finite barriers treated here. The number of bound states plus transmission resonances is again limited by the number of atoms in the quantum well. The barrier height can only affect the distribution of bound states versus resonances, not their total number. This is unlike the continuous model where the number of bound states always increases with barrier height and there are always transmission resonances above the well. As discussed below, this behaviour arises directly from the bulk bandstructure imposed by the discrete model.

Here the work in [2] on the infinite square well is extended to the finite square well in the discrete model, where semi-analytic solutions including graphical techniques are available. The present work goes far beyond that of [3] in several significant ways. First, we discuss not only the bound states of a symmetric well, but also the transmission resonances, where the boundary conditions are not symmetric; [3] does not treat this case at all. Second, we rely upon graphical techniques which are more closely tied to the treatment of the finite square well in the continuous model, so that our approach is much more accessible (for both faculty and students). Third, our discussion of the results in light of a physical bandstructure also enhances accessibility, and our formulation serves as a natural introduction to multi-band models of quantum wells. The limited treatment of only the bound states of a symmetric finite quantum well given in [3] does not so easily transfer to multi-band models. These extensions enhance the technological relevance, since now both bound states and transmission resonances can occur in the same structure. Section 2 discuses the discretized Schrödinger equation for the finite square well, first for bound states and second for the above-well transmission characteristic. Section 3 gives our conclusions.

2. Model and results

2.1. General

The discretized Schrödinger equation and its equivalent single-band tight-binding model are treated extensively in [1, 2], so its general properties are only briefly sketched here. The

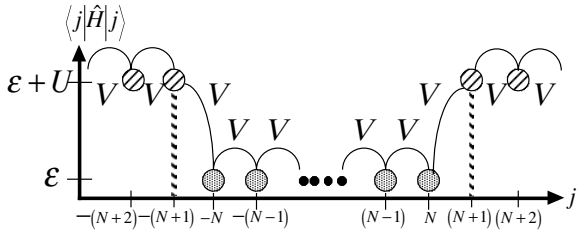

Figure 1. The finite quantum well in discrete quantum mechanics. The barrier height is U, and nearest-neighbour couplings are shown as links between atoms. Shaded atoms (indices $-N \leqslant j \leqslant N$) lie within the quantum well while striped atoms (indices $|j| \geqslant N+1$) lie within the barriers.

one-dimensional system studied is a chain of atoms along the z-axis, with inter-atomic spacing a. The quantum well is taken to occupy $2N+1$ sites, indexed $j = -N, \ldots, -1, 0, 1, \ldots, N$. The site indices in the barriers are $|j| \geqslant N+1$ (see figure 1). Each atom has a single s-like orbital, where the ket $|n\rangle$ is for the orbital on the atom of index n. The wavefunction is a superposition of these orbitals,

$$|\psi\rangle = \sum_{j=-\infty}^{+\infty} C_j |j\rangle, \tag{1}$$

where the C_j are expansion coefficients. The Hamiltonian is written as a sum of two operators, $\hat{H} = \hat{H}_0 + \hat{U}$, with matrix elements

$$\langle j'|\hat{H}|j\rangle = \varepsilon_s \delta_{j',j} + V[\delta_{j',j+1} + \delta_{j',j-1}] \tag{2}$$

$$\langle j'|\hat{U}|j\rangle = U_j \delta_{j',j} \tag{3}$$

$$U_j = \begin{cases} 0, & |j| \leqslant N \\ U, & |j| > N. \end{cases} \tag{4}$$

For exact correspondence with continuous quantum mechanics [15] in the appropriate limits, the on-site parameter, ε, and the nearest-neighbour parameter, V, are related:

$$V = -\frac{\hbar^2}{2m^* a^2}, \qquad \varepsilon = \frac{\hbar^2}{m^* a^2} = -2V, \tag{5}$$

where m^* is the effective mass (essentially the inverse curvature) of the conduction-band minimum. The Schrödinger equation in the tight-binding basis is a tridiagonal matrix equation (of infinite dimension) having rows:

$$\langle n|[\hat{H} - \hat{1}E]|\psi\rangle = VC_{n-1} + [\varepsilon + U_n - E]C_n + VC_{n+1} = 0. \tag{6}$$

Note that $V < 0, \varepsilon > 0$, and that the only difference between the barrier and well regions is the value of U_j.[3]

2.2. Physical and numerical viewpoints

Because equation (6) is mathematically identical to the discretized effective-mass Schrödinger equation, it may be viewed and presented as either an approximation to the continuous

[3] In general, ε and V could differ in the barrier and well. However, for exact correspondence with the familiar continuous space finite square well, corresponding on-site and nearest-neighbour parameters must be the same in both regions. Only the conduction-band offset, U_j, can differ.

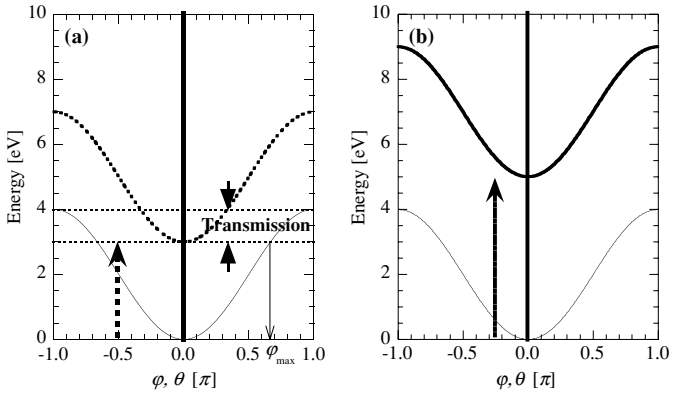

Figure 2. Bulk dispersions for the quantum well (thin solid line) and two different barrier materials (heavy lines; $\mu = U/2V$). The tight-binding parameters in both well and barriers are $\varepsilon = 2.0$ eV, $V = -1.0$ eV. Arrows indicate the two barrier heights. (a) $U = 3$ eV ($\mu = -1.5$) where transmission is possible for energies between the barrier minimum (3 eV) and the quantum well bulk maximum (4 eV). These energies are indicated by dotted lines and labelled 'transmission'. The quantum well phase corresponding to the barrier bulk minimum is indicated by $\varphi_{\max}$. (b) $U = 5$ eV ($\mu = -2.5$), where only bound states occur.

effective-mass Schrödinger equation or as a simple tight-binding model in its own right. While the mathematical equivalence of the discretized effective-mass Schrödinger equation and a simple tight-binding model has been previously noted [16], the physics implied by this equivalence is often not emphasized. This problem can thus be presented as part of either a numerical methods course or a solid-state physics course. Our emphasis here will mainly be on its use in a solid-state physics setting. However, since the numerical approach to this problem generally will be familiar to the broader physics and engineering community, we briefly outline how this problem might fit into a numerical methods class. After this brief discussion, we set forth our argument for its special relevance to solid-state physics.

Under the numerical viewpoint, three salient points emerge: the discretization scheme and choice of mesh points are not unique; the limit of zero mesh spacing is relevant and the cosine $E(k)$ relation shown in figure 2 is a numerical artefact [17–19], which follows on taking the limit $a \to 0$ in the bulk dispersion, equation (A.6), $E(k) \to \hbar^2 k^2/(2m^*)$. Within these bounds, two possible presentations naturally emerge. On one hand, the bulk dispersion, equation (A.6), might be found using Fourier factors in a manner similar to that employed in stability analysis [17, 19]. On the other hand, one might adopt an even deeper treatment, approaching equation (6) as a straightforward difference equation, whereupon application of periodic boundary conditions yields the bulk dispersion, equation (A.6). Reference [18] takes this approach in handling the problem of standing waves on a string fixed at both ends, which is mathematically equivalent to the infinite square well problem treated in [2]. Reference [20] treats physical problems with similar difference equations likewise having cosine dispersions. Regardless of the presentation, equation (A.6) is thus used only to ensure mathematical consistency in the computation of the energy eigenvalues and the major interest is showing that the lowest eigenvalues are most accurate [18]. Thus, in the numerical presentation the cosine dispersion is viewed as a 'numerical bandstructure', in analogy with the term 'numerical dispersion' employed in computational hydrodynamics [19].

While the numerical presentation has significant strengths, from here on we adopt a physical picture. We choose this approach for physical reasons only, not for reasons of taste. The most important of these concerns the derivation and nature of the effective-mass

Schrödinger equation itself. This differential equation in fact governs a slowly varying envelope, and is meaningless for lengths less than several lattice constants. Thus the limit $a \to 0$ for the discretized model is not physically justified, and it is therefore our position that the numerical view is best employed as a transition to the physical one.

In contrast, the physical presentation models an ideal crystal, with atoms placed at regular, finite intervals and finite same-atom and near-neighbour interactions. The atoms remain a finite distance apart, the nearest-neighbour interaction remains bounded and thus the limit $a \to 0$ is neither relevant nor allowed. The resulting energy bands are periodic and finite bandwidth, resembling much more closely the cosine curves of figure 2 than they do the parabolas of the continuous model. Because the matrix dimension is the major mathematical difference between single- and multi-band tight-binding calculations, the generalization to a multi-band model is simpler within a tight-binding context. In addition, because the tight-binding presentation uses a localized basis, it avoids confusion over issues such as inter-band or inter-valley scattering [9]. It is therefore our position that the best pedagogical presentation of the discretized Schrödinger equation is as a tight-binding model. Analytical tight-binding results can help the student connect the tight-binding presentation to more familiar results from the continuous treatment.

Establishing this connection is important since the bandwidth of the discrete model greatly affects the eigenstates of the finite well, just as it does those of the infinite well [2]. Figure 2 shows the resulting bulk dispersions of the two materials for two different values of offset, $U < 4|V|$ (figure 2(a), heavy dotted line) and $U > 4|V|$ (figure 2(b), heavy solid line) along with the quantum well dispersion (light solid line). In figure 2(a) the offset is less than the bandwidth ($U < 4|V|$), so the barrier lies below the quantum well bulk maximum. Above the region of bound states there is now a window of energy within which there are propagating states in both the barriers and well. Hence, this case has both bound states and transmission over the well. In figure 2(b) the offset is greater than the bandwidth ($U > 4|V|$), so that the barrier lies above the quantum well bulk maximum. Thus there are no propagating states at the same energy in both the barriers and well, and one finds only bound states. Experience with the infinite square well [2] suggests that the number of bound states (for $U > 4|V|$), or the number of bound states plus transmission resonances (for $U < 4|V|$) ought to be similarly limited here. These issues are addressed in the next two sub-sections.

2.3. Bound states

The bound state problem for the discretized Schrödinger equation shares characteristics with both its continuous counterpart and multi-band tight-binding models and therefore serves as a bridge between the two. For $U < 4|V|$, bound states occur in the range $0 < E < U$. In tight-binding terms this means they fall above the conduction-band minimum of the well and below that of the barrier, just as in the continuous model. For $U > 4|V|$ bound states occur in the range $0 < E < 4|V|$, independent of U, so that the conduction-band maximum in the well sets the upper limit, as can happen in multi-band models. Regardless, both the Hamiltonian and boundary conditions (decaying wavefunction in the barriers) are symmetric, and the potential is piecewise constant (zero in the well, U in the barriers). The wavefunction is thus a simultaneous eigenstate of parity and is a superposition of the bulk states of energy E in each region (well or barriers). These features are shared with the continuous model but often are not so clearly articulated.

Tight-binding approaches differ from the continuous treatment in the equations connecting the wavefunction across the interfaces and the manifestation of the essential physics (symmetry and a piecewise-constant potential). The parity symmetry appears in the wavefunction

coefficients C_j themselves, which are either even or odd. Likewise, the decay of the wavefunction in the barriers means that for $|j| > N$, $|C_j| \to 0$ as $|j| \to \infty$. The interface equations no longer involve derivatives, but are now just rows of the Schrödinger equation. As with the continuous case, only one interface need be considered because symmetry ensures that the pair on the left side is identical (up to a sign) to that on the right. The two rows of the Schrödinger equation linking the right side of the well to the right barrier read

$$VC_{N-1} + [\varepsilon - E]C_N + VC_{N+1} = 0 \tag{7}$$

$$VC_N + [\varepsilon + U - E]C_{N+1} + VC_{N+2} = 0. \tag{8}$$

As in multi-band models, the wavefunction expansion in terms of barrier or well bulk states involves matrix eigenvalues and eigenvectors, not continuous functions of position. In the quantum well $U_j = 0$, $j \in [-N, N]$, and the C_j are (even or odd) linear combinations of bulk states for the well material. These are complex exponentials [2] $\exp(\pm i\varphi j)$, with $0 \leqslant \varphi \leqslant \pi$. Thus, the coefficients are

$$C_j = C_0^{(e)} \cos(\varphi j), \qquad j = -N, \ldots, N \quad \text{even states,} \tag{9}$$

$$C_j = C_0^{(o)} \sin(\varphi j), \qquad j = -N, \ldots, N \quad \text{odd states,} \tag{10}$$

where $\varphi = ka$, k are the quantized wave vectors to be determined, and the $C_0^{(\alpha)}$ are normalization constants. Like the continuous model, once the quantized wave vectors k are known, the bound state energies follow on substitution of the k into the bulk dispersion for the quantum well material, given by equation (A.6).

It is in the wavefunction expansion in the barriers where the links to multi-band models become strongest, for finding the bulk states available at E involves solving a generalized, complex eigenproblem [8]. The derivations appear in the appendix of [2], and explicit solutions are given in section A.1 of the appendix of this paper. Here, there is only one decaying state at each $E < U$. In the right barrier one solves the forward eigenproblem ($C_{j+1} = \lambda C_j$), choosing the eigenvalue satisfying $|\lambda| < 1$; in the left barrier one solves the reverse eigenproblem ($C_{j-1} = \lambda C_j$), again choosing $|\lambda| < 1$. At the right barrier the boundary condition is

$$C_{N+2} = \lambda^{<} C_{N+1}^{(\alpha)}, \tag{11}$$

where the decaying eigenvalue $\lambda^{<}$ is given in equation (A.2); an analogous expression holds on the left side. The coefficients $C_{N+1}^{(\alpha)}$ are normalization constants, just like the $C_0^{(\alpha)}$ above.

Substituting equations (9) and (11) into equations (7) and (8) yields a system of two homogeneous equations for the even states; the corresponding system for the odd states follows on substitution of equations (10) and (11) into equations (7) and (8). The even-state system, after dividing out V (since $V \neq 0$) is

$$\begin{bmatrix} \cos[(N-1)\varphi] + \left(\frac{\varepsilon - E}{V}\right)\cos(N\varphi) & 1 \\ \cos(N\varphi) & \left(\frac{\varepsilon + U - E}{V}\right) + \lambda^{<} \end{bmatrix} \begin{bmatrix} C_0^{(e)} \\ C_{N+1}^{(e)} \end{bmatrix} = \begin{bmatrix} 0 \\ 0 \end{bmatrix}. \tag{12}$$

For non-trivial solutions to exist, the determinant of the matrix in equation (12) must vanish:

$$\left\{\cos[(N-1)\varphi] + \left(\frac{\varepsilon - E}{V}\right)\cos(N\varphi)\right\}\left\{\left(\frac{\varepsilon + U - E}{V}\right) + \lambda^{<}\right\} - \cos(N\varphi) = 0. \tag{13}$$

One finds the transcendental equation for the odd states in a similar manner; the result is

$$\left\{\sin[(N-1)\varphi] + \left(\frac{\varepsilon - E}{V}\right)\sin(N\varphi)\right\}\left\{\left(\frac{\varepsilon + U - E}{V}\right) + \lambda^{<}\right\} - \sin(N\varphi) = 0. \tag{14}$$

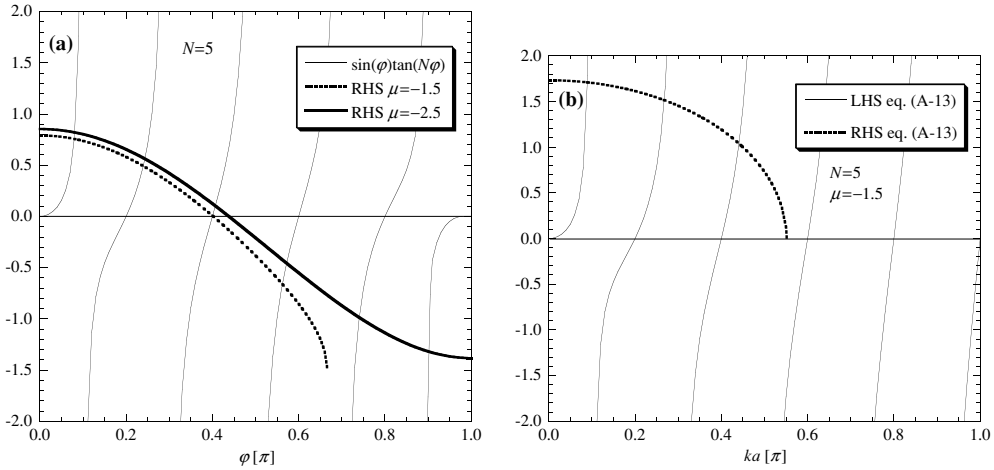

Figure 3. (a) Even-state determination for an 11 atom ($N = 5$) quantum well with either of the two barriers shown in figure 2. RHS refers to the right-hand side of equation (17). Each intersection corresponds to a bound state. (b) The even-state graph for the continuous case, equation (A.13) where $a = L/N$ and m^* are chosen to agree with the $N = 5$, $\mu = -1.5$ quantum well in the small k (or φ) limit. ka in (b) corresponds to φ in (a). Note that for higher barriers, there exist valid bound states for $ka > \pi$, unlike the discrete case of (a).

The even-state transcendental equation, equation (13), is greatly simplified by expanding $\cos[(N-1)\varphi]$, dividing out $\cos(N\varphi)$ and employing equation (A.5) to replace the term in the second pair of curly braces:

$$\left[\cos(\varphi) + \sin(\varphi)\tan(N\varphi) + \left(\frac{\varepsilon - E}{V}\right)\right]\left(-\frac{1}{\lambda^<}\right) - 1 = 0. \tag{15}$$

Equation (15) is further simplified by: (i) using equation (A.6) to rewrite $\cos(\varphi) = (E - \varepsilon)/2V$, then rearranging; (ii) multiplying through by $-\lambda^<$, then using equation (A.2); (iii) introducing the dimensionless well position (relative to the barrier) μ,

$$\mu = \frac{U}{2V}; \tag{16}$$

and (iv) using equation (A.6) and $\sin^2(\varphi) + \cos^2(\varphi) = 1$ in the square root of equation (A.2). Since $\mu < 0$, deeper wells correspond to more negative μ; for $\mu < -2$ the quantum well bulk maximum falls below the barrier bulk minimum. These simplifications give

$$\sin(\varphi)\tan(N\varphi) = \mu + \sqrt{\mu^2 - 2\mu\cos(\varphi) - \sin^2(\varphi)}. \tag{17}$$

Similar manipulations yield the odd-state transcendental equation:

$$-\sin(\varphi)\cot(N\varphi) = \mu + \sqrt{\mu^2 - 2\mu\cos(\varphi) - \sin^2(\varphi)}. \tag{18}$$

Equations (17) and (18) appear somewhat different from their counterparts in continuous quantum mechanics [15], however, as shown in subsection A.3 of the appendix, they have the correct continuous limits.

The differences between transcendental equations (17) and (18) and their conventional quantum mechanics counterparts, equations (A.13) and (A.14), are significant and lead to interesting new physics. These differences are easily seen in the graphical solution of equations (17) and (18), figures 3(a) and 4. For comparison, the even solutions for the continuous limit of the case $N = 5$, $\mu = -1.5$ are graphed in figure 3(b). Most notably,

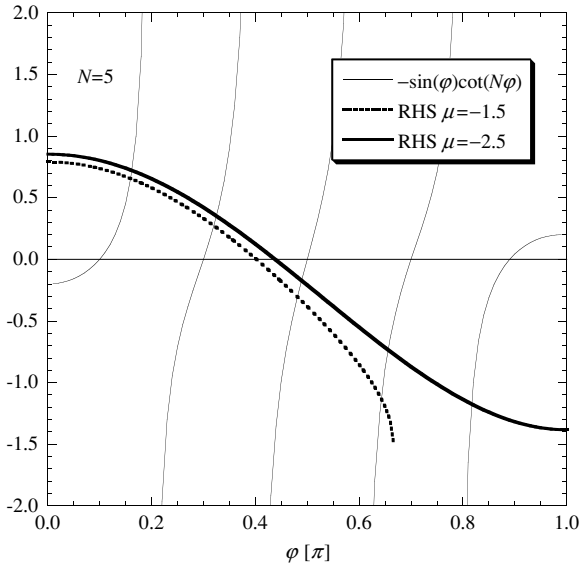

Figure 4. Odd-state determination for an 11 atom ($N = 5$) quantum well with either of the two barriers shown in figure 2. RHS refers to the right-hand side of equation (18). Each intersection corresponds to a bound state.

since $\mu < 0$, the negative portion of the graphs of $\sin(\varphi)\tan(N\varphi)$ and $-\sin(\varphi)\cot(N\varphi)$ are now accessible, and lead to valid solutions. Furthermore, expansion of the square root in equations (17) and (18) shows that for $\mu \leqslant -2$ the right-hand side never becomes imaginary over the domain of $0 \leqslant \varphi \leqslant \pi$. This assertion follows from examining the zeros of the argument of the root in equations (17) and (18):

$$\mu^2 - 2\mu\cos(\varphi) - \sin^2(\varphi) = (\mu^2 - 1) - 2\mu\cos(\varphi) + \cos^2(\varphi) = 0 \tag{19}$$

$$\cos(\varphi) = \tfrac{1}{2}\left[2\mu + \sqrt{4\mu^2 - 4\mu^2 + 4}\right] = \mu + 1, \tag{20}$$

where equation (20) is the only root with real solutions φ since $\mu < 0$. For $\mu < -2$ there are no real solutions of equation (19) at all, and the square root in equations (17) and (18) remains real. Consequently, there will be intersections with each segment of the left-hand side of equation (17) or (18).

From this last observation one concludes that for $\mu < -2$ there are always $(2N + 1)$ bound states, one per atom in the well, just as one finds in the case of infinite barriers [2]. Mathematically, this is demonstrated by noting that the zeros of $\sin(\varphi)\tan(N\varphi)$ occur at

$$\varphi_z = \frac{2n\pi}{2N}, \qquad n = 0, 1, \ldots, N \tag{21}$$

while those of $-\sin(\varphi)\cot(N\varphi)$ occur at

$$\varphi_z = \frac{(2n+1)\pi}{2N}, \qquad n = 0, 1, \ldots, N-1. \tag{22}$$

In addition, each segment of either plot is negative to the left of a zero and positive to the right of it, since for $\delta > 0, \delta \ll 1$, trigonometric identities show that $\tan[N(2n\pi/2N \pm \delta/N)] = \pm\tan(\delta)$ and $-\cot[N(2(n+1)\pi/2N \pm \delta/N)] = \pm\cot(\delta)$, while $\sin(\varphi) > 0$ over the domain $0 \leqslant \varphi \leqslant \pi$. Hence, when $\mu < -2$ the square root in equations (17) and (18) is real over the entire domain, so that the right-hand side will intersect each of these segments once, $N + 1$

times with the even-state curve, and N times with the odd-state curve, for a total of $2N + 1$ intersections and hence $2N + 1$ bound states. This observation also has been found in [3], but in a purely mathematical and largely analysis-based (as opposed to graphical) treatment. This mathematical fact is due to the significant underlying physics.

The physical significance of this fact is apparent from the energy band diagram, figure 2. When $\mu < -2$ the band minimum of the barrier lies above the band maximum of the well (e.g., the $\mu = -2.5$ curve in figure 2(b)). Because there are no bulk Bloch states above the band maximum there are no bound states between the bulk band maximum in the quantum well and the bulk band minimum in the barrier. The number of bound states increases with the barrier height until the barrier exceeds the quantum well bulk band maximum ($U > -4V$), at which point there are $(2N + 1)$ bound states. This number of bound states is unchanged as the barrier is raised beyond this point. This behaviour is very different from conventional quantum mechanics [15] where the number of bound states continually increases with the barrier height. The reason for the difference between the continuous and discrete models is the dissimilar $E(k)$ dispersion in the two. As discussed in [2], the continuous model has a purely parabolic dispersion (i.e., no maximum), so that there are propagating states in the well at all energies above the minimum. In contrast, the discrete model has a finite bandwidth in which solutions exist.

Figures 3(a) and 4 illustrate the bound state solutions for a quantum well of 11 atoms ($N = 5$). Figure 3(a) graphs the even-state equation and figure 4 the odd-state equation; in both figures the abbreviation 'RHS' denotes the right-hand side of equations (17) and (18) as appropriate. Note that for $\mu = -2.5$, the right-hand side is real over the entire domain and there are indeed intersections with all segments of both curves: six (6) even and five (5) odd states, for a total of 11 bound states. For $\mu = -1.5$, the square root in equations (17) and (18) becomes imaginary at $\varphi = 2\pi/3$ and the curve terminates, so that there are no intersections with the last two segments of the even-state curve and the final segment of the odd-state curve. Thus, there are only four (4) bound even states and four (4) bound odd states for a total of eight (8) bound states. The continuous limit of this case (figure 3(b)) has only three (3) bound even states mainly because its transcendental equation has no negative offset. The following subsection extends the treatment to the quasi-bound states (transmission resonances) lying above the barrier bulk minimum.

2.4. Transmission characteristics

Interesting transmission characteristics occur when $-2 < \mu < 0$ and $U < E < -4V$, a case not treated in [3]. Here the barrier bulk minimum lies below the quantum well bulk maximum and the energy of the carrier falls between these two points (e.g., the $\mu = -1.5$ curve in figure 2). Hence there are propagating states in the barrier, and the bulk dispersion there is given in equation (A.7). The carrier speeds are proportional to $|\mathrm{d}E/\mathrm{d}k| = 2a|V|\sin(\theta)$ and are identical in the left and right barriers since the barriers are symmetric. Thus, the flux ratios reduce to ratios of the square magnitudes of amplitudes.

The transmission problem involves a carrier incident from the left (negative index) barrier region in a state of definite K incident on the quantum well, transmitting over it into a state of the same K in the right barrier region. The rows of the Schrödinger equation on the transmitted (right) side are

$$VC_{N-1} + [\varepsilon - E]C_N + VC_{N+1} = 0 \tag{23}$$

$$VC_N + [\varepsilon + U - E]C_{N+1} + VC_{N+2} = 0. \tag{24}$$

Those on the incident/reflected (left) side are

$$VC_{-(N+2)} + [\varepsilon + U - E]C_{-(N+1)} + VC_{-N} = 0 \tag{25}$$

$$VC_{-(N+1)} + [\varepsilon - E]C_{-N} + VC_{-(N-1)} = 0, \tag{26}$$

where the C_j are no longer of definite parity since the boundary conditions to be applied are not symmetric.

As discussed in [2], the coefficients inside the quantum well are superpositions of Bloch coefficients:

$$C_j = A\,\mathrm{e}^{\mathrm{i}\varphi j} + B\,\mathrm{e}^{-\mathrm{i}\varphi j}, \qquad j = -N, \ldots, (N-1), N, \tag{27}$$

where $\varphi = ka$ as in appendix A.2. On the transmitted side, $j \geqslant N+1$, there is only a single forward propagating state. Its coefficient is set to the transmission amplitude at the interface:

$$C_{N+1} = T, \qquad C_{N+2} = T\,\mathrm{e}^{\mathrm{i}\theta}, \tag{28}$$

where $\theta = Ka$ as in appendix A.2 and the second of equations (28) follows from the Bloch relation [2] $C_{j+1} = \mathrm{e}^{\mathrm{i}Ka}C_j$. On the incident/reflected side, $j \leqslant -(N+1)$, the coefficients are a superposition of a unit amplitude, forward propagating, incident state and a reflected, reverse-propagating state, amplitude R:

$$C_{-(N+1)} = 1 + R, \qquad C_{-(N+2)} = \mathrm{e}^{-\mathrm{i}\theta} + R\,\mathrm{e}^{\mathrm{i}\theta}, \tag{29}$$

where again $\theta = Ka$ and the Bloch relation [2] for the incident state is $C_j = \mathrm{e}^{-\mathrm{i}Ka}C_{j+1}$ while that for the reflected state is $C_j = \mathrm{e}^{\mathrm{i}Ka}C_{j+1}$.

The transmission and reflection amplitudes are found by substituting equations (27)–(29) into equations (23)–(26) and eliminating the quantum well coefficients A and B. This process is facilitated by using bulk relation equations (A.6) and (A.7) to rewrite $\varepsilon - E = -2V\cos(\varphi)$ and $\varepsilon + U - E = -2V\cos(\theta)$. After some trigonometry and simplification ($V \neq 0$), equations (23) and (24) become

$$\begin{bmatrix} \mathrm{e}^{\mathrm{i}(N+1)\varphi} & \mathrm{e}^{-\mathrm{i}(N+1)\varphi} \\ \mathrm{e}^{\mathrm{i}N\varphi} & \mathrm{e}^{-\mathrm{i}N\varphi} \end{bmatrix} \begin{bmatrix} A \\ B \end{bmatrix} = T \begin{bmatrix} 1 \\ \mathrm{e}^{\mathrm{i}\theta} \end{bmatrix} \tag{30}$$

while equations (25) and (26) become

$$\begin{bmatrix} \mathrm{e}^{-\mathrm{i}(N+1)\varphi} & \mathrm{e}^{\mathrm{i}(N+1)\varphi} \\ \mathrm{e}^{-\mathrm{i}N\varphi} & \mathrm{e}^{\mathrm{i}N\varphi} \end{bmatrix} \begin{bmatrix} A \\ B \end{bmatrix} = \begin{bmatrix} 1 + R \\ \mathrm{e}^{\mathrm{i}\theta} + R\,\mathrm{e}^{-\mathrm{i}\theta} \end{bmatrix}. \tag{31}$$

Equation (30) is easily solved for A and B by matrix inversion. The result is then substituted into equation (31), which is then rearranged to give a pair of two linear equations in R and T. Once again, the system is easily solved by matrix inversion and the resulting transmission and reflection coefficients are found:

$$|T|^2 = \frac{1}{1 + \sin^2[(2N+1)\varphi][\cot(\theta)\,\mathrm{cosec}(\varphi) - \cot(\varphi)\,\mathrm{cosec}(\theta)]^2} \tag{32}$$

$$|R|^2 = \frac{\sin^2[(2N+1)\varphi][\cot(\theta)\,\mathrm{cosec}(\varphi) - \cot(\varphi)\,\mathrm{cosec}(\theta)]^2}{1 + \sin^2[(2N+1)\varphi][\cot(\theta)\,\mathrm{cosec}(\varphi) - \cot(\varphi)\,\mathrm{cosec}(\theta)]^2}. \tag{33}$$

Note that flux is conserved: $|R|^2 + |T|^2 = 1$. As with the bound states, these two equations at first seem to differ from their counterparts in conventional quantum mechanics [15]. However, as shown in appendix A.4, equations (32) and (33) do indeed have the correct limits.

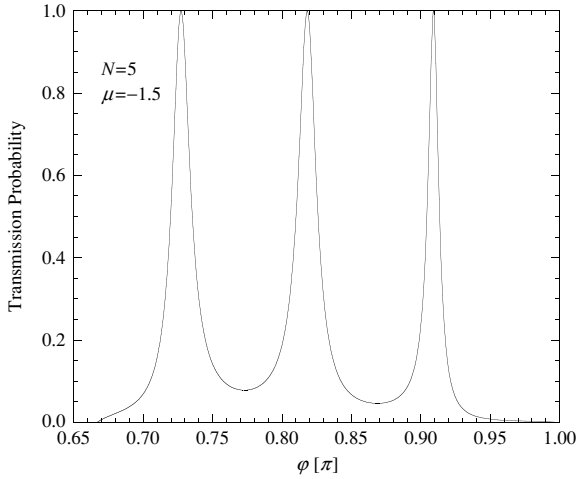

Figure 5. Transmission probability versus phase in the quantum well for an 11 atom ($N = 5$) quantum well and the $\mu = -1.5$ barriers. The transmission is unity at three points, given by equation (34) for $m = 8, 9, 10$.

In equation (32) observe that the transmission probability becomes unity at certain values of φ called transmission resonances,

$$\varphi_{\text{res}}(m) = \frac{m\pi}{2N+1}, \qquad m = m_{\min}, \ldots, 2N-1, 2N, \tag{34}$$

where $m_{\min}$ is the smallest integer such that[4] $E(\varphi_{\text{res}}(m_{\min})) > U$. Figure 5 graphs a typical transmission characteristic, here for transmission over an 11-atom ($N = 5$) quantum well for $\mu = -1.5$. As expected from equations (32) and (34), the transmission is unity for $m = 8, 9, 10$. As noted in subsection 2.2 (figures 3(a) and 4), this quantum well has eight (8) bound states, so that the total number of bound states and transmission resonances is 11, the same as the number of atoms in the well. This fact is no coincidence. Instead, it is very general, as shown below.

Consider first the case in which the last (i.e., highest energy) bound-state intersection occurs with the even-state curve, in the section $n = n_0$. From equation (21), the right-hand side of equation (17) intersects the even-state curve for $n = 0, 1, \ldots, n_0$, giving a total of $(n_0 + 1)$ bound even states. In addition, the right-hand side of equation (18) must likewise intersect all odd-state segments with zeros less than $2\pi n_0/2N$. From equation (22) these are the segments $n = 0, 1, \ldots, n_0 - 1$, giving a total of n_0 bound odd states. As shown below, the first transmission resonance is that for which $\varphi_{\text{res}} > 2\pi n_0/2N$. Thus,

$$\frac{m_{\min}\pi}{2N+1} - \frac{2n_0\pi}{2N} > 0 \tag{35}$$

$$Nm_{\min} - n_0(2N+1) > 0 \tag{36}$$

$$m_{\min} > 2n_0 + \frac{n_0}{N}. \tag{37}$$

Since for transmission resonances $n_0 < N$ ($n_0 = N$ implies all bound states), $m_{\min} = 2n_0 + 1$. Transmission resonances therefore occur for $m = 2n_0 + 1, \ldots, 2N - 1, 2N$, giving a

[4] The case $m = 2N + 1 \Rightarrow \varphi = \pi$ does not represent a transmission resonance because both $\text{cosec}(\varphi)$ and $\cot(\varphi)$ diverge. Taking the limit $\varphi \to \pi$, one finds for the transmission coefficient $|T|^2 \to 1/\{1 + (2N + 1)^2[\cot(\theta) + \text{cosec}(\theta)]^2\}$, which is less than unity.

total of $2N - 2n_0$ resonances. The number of resonances plus bound states is therefore $n_0 + 1 + n_0 + 2N - 2n_0 = 2N + 1$, the number of atoms in the well.

If on the other hand the last (i.e., highest energy) bound-state intersection occurs with the odd-state curve in the section $n = n_0$, by equation (22) there are clearly odd-state intersections for $n = 0, 1, \ldots, n_0$ giving a total of $(n_0 + 1)$ bound odd states. Furthermore, the right-hand side of equation (17) must intersect all even-state segments with zeros less than $(2n_0 + 1)\pi/2N$, i.e., those for $n = 0, 1, \ldots, n_0$, so that there are also $(n_0 + 1)$ bound even states. The first transmission resonance for which $\varphi_{\text{res}} > (2n_0 + 1)\pi/2N$ is found by requiring:

$$\frac{m_{\min}\pi}{2N+1} - \frac{(2n_0+1)\pi}{2N} > 0 \tag{38}$$

$$2Nm_{\min} - (2n_0 + 1)(2N + 1) > 0 \tag{39}$$

$$m_{\min} > (2n_0 + 1)\left(1 + \frac{1}{2N}\right) = 2n_0 + 1 + \frac{2n_0 + 1}{2N}. \tag{40}$$

Since $n_0 < N - 1$, $(2n_0 + 1)/2N < 1$, and hence $m_{\min} = 2n_0 + 2$. The transmission resonances therefore occur for $m = 2n_0 + 2, \ldots, 2N - 1, 2N$, giving $2N - 2n_0 - 1$ resonances. The total number of bound states and resonances is the same as before since $2N - 2n_0 - 1 + 2(n_0 + 1) = 2N + 1$, the number of atoms in the well.

The only assertion in the above proof which remains to be verified is that concerning the first resonance. Specifically, it must be demonstrated that this resonance occurs after the zero of the last segment of the left-hand side of equations (17) or (18) containing an intersection. This assertion can be verified by demonstrating that the next-lower candidate resonance occurs at energy $E < U$, that is, below the barrier bulk minimum, and hence is in the region of bound states (there are no propagating states in the barriers for $E < U$). The quantum well bulk phase corresponding to the barrier bulk minimum, denoted by $\varphi_{\max}$ (figure 2), is found by setting $E(\varphi_{\max}) = U$ in equation (A.6), yielding

$$\cos(\varphi_{\max}) = 1 + \mu. \tag{41}$$

Substituting equation (41) into the right-hand side of equation (17) or (18) gives

$$\mu + \sqrt{\mu^2 - 2\mu\cos(\varphi_{\max}) - \sin^2(\varphi_{\max})} = \mu = \cos(\varphi_{\max}) - 1. \tag{42}$$

If the last intersection is with the segment $n = n_0$ of the even-state curve, the highest energy at which this can occur is obviously just below the barrier bulk minimum, $E = U^-$, or $\varphi = \varphi_{\max}$. This implies that $(2n_0 - 1)\pi/2N < \varphi_{\max} < 2n_0\pi/2N$. Substituting equations (41) and (42) into the even-state equation (17) gives

$$\sin(\varphi_{\max})\tan(N\varphi_{\max}) = \cos(\varphi_{\max}) - 1. \tag{43}$$

Equation (43) is simplified with standard trigonometric relations to yield

$$\cos[(N+1)\varphi_{\max}] - \cos(N\varphi_{\max}) = -2\sin\left(\frac{\varphi_{\max}}{2}\right)\sin\left[\frac{(2N+1)}{2}\varphi_{\max}\right] = 0. \tag{44}$$

Equation (44), together with the bounds on $\varphi_{\max}$ imply that

$$\varphi_{\max} = \frac{2n_0\pi}{2N+1}, \tag{45}$$

in other words, that $\varphi_{\max} = \varphi_{\text{res}}(2n_0)$. Since $\varphi_{\max}$ is the phase of a bound state, so too is $\varphi_{\text{res}}(2n_0)$, and therefore it cannot be a transmission resonance. Note that for μ slightly more negative than the critical value (i.e., a slightly higher barrier), the candidate resonance $\varphi_{\text{res}}(2n_0)$ moves further below the bulk band minimum.

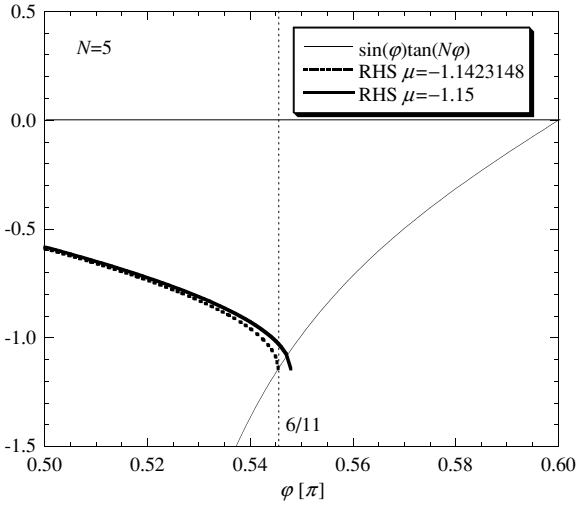

Figure 6. Graphical construction for the proof that the potential resonance below the zero of the last intersecting segment lies in the regime of bound states, and hence is not a transmission resonance at all (see the text).

Figure 6 illustrates a geometric construction of the above proof for the 11 atom ($N = 5$) quantum well; the right-hand side of equation (17) is graphed for two different values of μ. There are even bound states for $n = 0, 1, 2, 3$, since the last intersection is with the even-state segment $n = 3$. When $\mu \approx -1.1423$ the intersection just barely occurs, at phase $\varphi_{\max} = 6\pi/11$, as indicated by equation (45). For $\mu = -1.15$ the intersection occurs at a slightly greater phase (slightly higher energy), and, as claimed above, the candidate resonance $\varphi_{\text{res}} = 6\pi/11$ falls below the barrier bulk minimum, into the regime of bound states, not transmission resonances.

A similar proof holds when the final intersection occurs with the odd-state graph segment $n = n_0$. Again, consider the case of a barely bound state, $E = U^-$, or $\varphi = \varphi_{\max}$. This implies that $2n_0\pi/2N < \varphi_{\max} < (2n_0 + 1)\pi/2N$. Substituting equations (41) and (42) into equation (18) gives

$$-\sin(\varphi_{\max})\cot(N\varphi_{\max}) = \cos(\varphi_{\max}) - 1. \tag{46}$$

Equation (46) is simplified with standard trigonometric relations to yield

$$\sin[(N+1)\varphi_{\max}] - \sin(N\varphi_{\max}) = 2\sin\left(\frac{\varphi_{\max}}{2}\right)\cos\left[\frac{(2N+1)}{2}\varphi_{\max}\right] = 0. \tag{47}$$

Just as with the even-state case above, the cosine in equation (47) must vanish, so that

$$\varphi_{\max} = \frac{(2n_0 + 1)\pi}{2N + 1}. \tag{48}$$

Thus, when the last bound state is odd and lies just below the barrier bulk minimum its phase is $\varphi_{\max} = \varphi_{\text{res}}(2n_0 + 1)$. Again, for slightly more negative μ (slightly deeper well), the candidate resonance $\varphi_{\text{res}}(2n_0 + 1)$ falls further below the bulk band minimum, in the regime of bound states, not transmission resonances. Thus, in all cases the first transmission resonance is that immediately following the zero of the last intersecting segment.

Although the proof assumes that the final intersection occurs in the negative half of the graph, the results also hold if the final intersection occurs in the positive half. If the last intersection is with the even-state curve, then the highest bound state must lie below

$\varphi_{\rm res}(2n_0+1)$, since equation (48) shows that if it were higher than $\varphi_{\rm res}(2n_0+1)$ the final intersection would be with the odd-state curve, contrary to the assumption. Likewise, if the final intersection is with the odd-state curve, then the bound state must fall below $\varphi_{\rm res}(2n_0)$, since equation (45) shows that if it were higher than $\varphi_{\rm res}(2n_0)$ the final intersection would be with the even-state curve, again contrary to the assumption.

3. Conclusions

The finite square well as treated in discretized quantum mechanics differs significantly from its more familiar counterpart from continuous quantum mechanics. This fundamentally different physics arises directly from the finite bandwidth of the discrete model. If the barrier bulk minimum is above the quantum well bulk maximum (i.e., barrier height greater than the bandwidth), there are only bound states, and there is one state for each atom in the quantum well. If on the other hand the barrier height is less than the bandwidth (i.e., barrier bulk minimum below the quantum well bulk maximum) transmission resonances are also possible, and the number of bound states plus the number of transmission resonances again equals the number of atoms in the quantum well. Due to its finite bandwidth and energy-dependent effective mass, the discrete model is much more representative of the bandstructure of true solids and thus illuminates results from more complete, full-bandstructure models.

Acknowledgment

GF acknowledges the support of the National Science Foundation, grant no EEC-0228390.

Appendix

A.1. Forward- and reverse-eigenproblems

The forward ($C_{j+1}=\lambda C_j$) and reverse ($C_{j-1}=\lambda C_j$) eigenproblems are derived in the appendix of [2]; both yield the same characteristic polynomial. Here these eigenproblems are solved for the barrier regions, where the characteristic polynomial is

$$\lambda^2+\left(\frac{\varepsilon+U-E}{V}\right)\lambda+1=0. \tag{A.1}$$

For $E<U$ one root decays going into the barrier, the other grows. The physically relevant, decaying root, which ensures that $|C_j|\to 0$ as $|j|\to\infty$ for $|j|>N$, is denoted by $\lambda^<$:

$$\lambda^<=-\left(\frac{\varepsilon+U-E}{2V}\right)-\sqrt{\left(\frac{\varepsilon+U-E}{2V}\right)^2-1}. \tag{A.2}$$

That this eigenvalue has magnitude less than unity follows from the fact that $V<0$ and $E<U$. While not physically relevant, the growing eigenvalue, denoted by $\lambda^>$, is useful for simplifying equations via its relationship to the decaying eigenvalue:

$$\lambda^>=-\left(\frac{\varepsilon+U-E}{2V}\right)+\sqrt{\left(\frac{\varepsilon+U-E}{2V}\right)^2-1}. \tag{A.3}$$

Equations (A.2) and (A.3) lead to two useful results:

$$\lambda^<\lambda^>=1\Rightarrow\lambda^>=\frac{1}{\lambda^<}, \tag{A.4}$$

$$\lambda^{<} + \left(\frac{\varepsilon + U - E}{V}\right) = -\lambda^{>} = -\frac{1}{\lambda^{<}}. \tag{A.5}$$

A.2. Bulk dispersions

The dispersions for the bulk materials comprising the quantum well and barriers are also of use. Equation (11) of [2] derives the bulk dispersion for the well ($U = 0$),

$$E = \varepsilon + 2V\cos(\varphi), \qquad \varphi = ka, \tag{A.6}$$

where the phase is restricted to the first Brillouin zone, $-\pi < \varphi \leqslant \pi$. For calculating transmission characteristics ($E > U$), the bulk dispersion of the barrier material is also relevant, and is trivially obtained from equation (A.6) by replacing $\varepsilon \to \varepsilon + U$,

$$E = \varepsilon + U + 2V\cos(\theta), \qquad \theta = Ka, \tag{A.7}$$

where once again $-\pi < \theta \leqslant \pi$. Note that the wave vectors k and K are different.

A.3. Continuous limits of the bound-state equations

Equations (17) and (18) appear different from their counterparts in continuous quantum mechanics. Nevertheless, they do have the proper limit, in which the number of lattice points (atoms) becomes infinite, the spacing between them infinitesimal while the quantum well length remains constant and finite: $a \to 0$, $N \to \infty$, $aN = L$. To demonstrate this limit, first divide equation (17) by a:

$$\frac{1}{a}\sin(\varphi)\tan(N\varphi) = \frac{\mu}{a} + \sqrt{\left(\frac{\mu}{a}\right)^2 - 2\frac{\mu}{a^2}\cos(\varphi) - \frac{1}{a^2}\sin^2(\varphi)}. \tag{A.8}$$

Using $\varphi = ka$, the left-hand side of equation (A.8) has the limit:

$$\lim_{\substack{a\to 0, N\to\infty, \\ aN=L}} \left[\frac{1}{a}\sin(\varphi)\tan(N\varphi)\right] = k\tan(Lk). \tag{A.9}$$

The limits of μ/a and μ/a^2 are needed to evaluate the limit of the right-hand side of equation (A.8) and are found on substituting equation (5) into equation (16):

$$\lim_{\substack{a\to 0, N\to\infty, \\ aN=L}} \left[\frac{\mu}{a}\right] = \lim_{\substack{a\to 0, N\to\infty, \\ aN=L}} \left[\frac{-Um^*a}{\hbar^2}\right] = 0, \tag{A.10}$$

$$\lim_{\substack{a\to 0, N\to\infty, \\ aN=L}} \left[\frac{\mu}{a^2}\right] = \lim_{\substack{a\to 0, N\to\infty, \\ aN=L}} \left[\frac{-Um^*}{\hbar^2}\right] = \frac{-Um^*}{\hbar^2}. \tag{A.11}$$

Thus, the limit of the right-hand side of equation (A.8) is

$$\lim_{\substack{a\to 0, N\to\infty \\ aN=L}} \left[\frac{\mu}{a} + \sqrt{\left(\frac{\mu}{a}\right)^2 - 2\frac{\mu}{a^2}\cos(\varphi) - \frac{1}{a^2}\sin^2(\varphi)}\right] = \sqrt{\frac{2m^*U}{\hbar^2} - k^2}, \tag{A.12}$$

so that in continuous quantum mechanics transcendental equation (17) becomes

$$k\tan(Lk) = \sqrt{\frac{2m^*U}{\hbar^2} - k^2}. \tag{A.13}$$

Equation (A.13) agrees with the even-state transcendental equation for the finite quantum well in continuous quantum mechanics [15]. Similar manipulations give the limit of odd-state transcendental equation (18),

$$-k\cot(Lk) = \sqrt{\frac{2m^*U}{\hbar^2} - k^2}, \tag{A.14}$$

which is again the same as found in conventional quantum mechanics [15].

A.4. Continuous limit of transmission characteristics

Equations (32) and (33) differ from their counterparts in continuous quantum mechanics [15], yet they do have the correct limits. Here one takes $a \to 0,\ N \to \infty,\ a(2N+1) = 2L$, so that as the number of mesh points becomes infinite, and the mesh spacing infinitesimal, the quantum well length remains constant. In this limit, one immediately finds $\sin^2[(2N+1)\varphi] \to \sin^2(2kL)$. For the remaining terms, it is useful to recall that as $a \to 0,\ \varphi \to 0,\ \theta \to 0$, and applying L'Hôpital's rule twice:

$$\frac{\cot(\varphi)}{\sin(\theta)} - \frac{\cot(\theta)}{\sin(\varphi)} = \frac{\cos(\varphi) - \cos(\theta)}{\sin(\theta)\sin(\varphi)} \tag{A.15}$$

$$\lim_{a\to 0}\left[\frac{\cos(\varphi) - \cos(\theta)}{\sin(\theta)\sin(\varphi)}\right] = \lim_{a\to 0}\left[\frac{-k\sin(\varphi) + K\sin(\theta)}{K\cos(\theta)\sin(\varphi) + k\cos(\varphi)\sin(\theta)}\right] \tag{A.16}$$

$$\lim_{a\to 0}\left[\frac{\cos(\varphi) - \cos(\theta)}{\sin(\theta)\sin(\varphi)}\right] = \lim_{a\to 0}\left[\frac{-k^2\cos(\varphi) + K^2\cos(\theta)}{2kK\cos(\theta)\cos(\varphi) - (k^2+K^2)\sin(\varphi)\sin(\theta)}\right] \tag{A.17}$$

$$\lim_{a\to 0}\left[\frac{\cos(\varphi) - \cos(\theta)}{\sin(\theta)\sin(\varphi)}\right] = \frac{K^2 - k^2}{2Kk} = \frac{1}{2}\left(\frac{K}{k} - \frac{k}{K}\right). \tag{A.18}$$

Thus,

$$\lim_{\substack{a\to 0, N\to\infty,\\ a(2N+1)=L}} |T|^2 = \frac{1}{1 + (1/4)\sin^2(2kL)\,(K/k - k/K)^2} \tag{A.19}$$

$$\lim_{\substack{a\to 0, N\to\infty,\\ a(2N+1)=L}} |R|^2 = \frac{(1/4)\sin^2(2kL)\,(K/k - k/K)^2}{1 + (1/4)\sin^2(2kL)\,(K/k - k/K)^2} \tag{A.20}$$

which agree with what one finds in conventional quantum mechanics [15].

References

[1] Boykin T B 2001 Tight-binding-like expressions for the continuous-space electromagnetic coupling Hamiltonian *Am. J. Phys.* **69** 793–8

[2] Boykin T B and Klimeck G 2004 The discretized Schrödinger equation and simple models for semiconductor quantum wells *Eur. J. Phys.* **25** 503–14

[3] Juang J, Lin W-W and Shieh S-F 2001 Eigenvalue problems for one-dimensional discrete Schrödinger operators with symmetric boundary conditions *SIAM J. Matrix Anal. Appl.* **23** 524–33

[4] DiCarlo A 2003 Microscopic theory of nanostructured semiconductor devices: beyond the envelope-function approximation *Semicond. Sci. Technol.* **18** R1–31

[5] Pecchia A and Di Carlo A 2004 Atomistic theory of transport in organic and inorganic nanostructures *Rep. Prog. Phys.* **67** 1497–561

[6] Di Carlo A and Lugli P 1995 Valley mixing in resonant tunneling diodes with applied hydrostatic pressure *Semicond. Sci. Technol.* **10** 1673–9

[7] Strahberger C and Vogl P 2000 Model of room-temperature resonant-tunneling current in metal/insulator and insulator/insulator heterostructures *Phys. Rev.* B **62** 7289–97

[8] Boykin T B 1996 Generalized eigenproblem method for surface and interface states: the complex bands of GaAs and AlAs *Phys. Rev.* B **54** 8107–15
Boykin T B 1996 Tunneling calculations for systems with singular coupling matrices: results for a simple model *Phys. Rev.* B **54** 7670–3

[9] Boykin T B, van der Wagt J P A and Harris J S Jr 1991 Tight-binding model for GaAs/AlAs resonant-tunneling diodes *Phys. Rev.* B **43** 4777–84

[10] Mamaluy D, Sabathil M and Vogl P 2003 Efficient method for the calculation of ballistic quantum transport *J. Appl. Phys.* **93** 4628–33

[11] Graf M and Vogl P 1995 Electromagnetic field and dielectric response in empirical tight-binding theory *Phys. Rev.* B **51** 4940–9

[12] Boykin T B, Bowen R C and Klimeck G 2001 Electromagnetic coupling and gauge invariance in the empirical tight-binding method *Phys. Rev.* B **63** 245314
[13] Boykin T B and Vogl P 2002 Dielectric response of molecules in empirical tight-binding theory *Phys. Rev.* B **65** 035202
[14] Vogl P, Hjalmarson H P and Dow J D 1983 A semi-empirical tight-binding theory of the electronic structure of semiconductors *J. Phys. Chem. Solids* **44** 365–78
[15] See, for example, Schwabl F 1992 *Quantum Mechanics* (New York: Springer) chapter 3
[16] Datta S 1995 *Electronic Transport in Mesoscopic Systems* (New York: Cambridge University Press) section 3.5
[17] Press W H, Flannery B P, Teukolsky S A and Vetterling W T 1992 *Numerical Recipes in C* 2nd edn (New York: Cambridge University Press) section 19.1
[18] Fried I 1979 *Numerical Solution of Differential Equations* (New York: Academic) sections 6.2–6.3
[19] Lele S K 1992 Compact finite difference schemes with spectral-like resolution *J. Comput. Phys.* **103** 16–42
[20] Levy H and Lessman F 1961 *Finite Difference Equations* (New York: Dover) chapters 4, 7